



## NOTICES

When U. S. Government drawings specifications, or other data are used for any purpose other than a definitely related Government procurement operation, the Government thereby incurs no responsibility nor any obligation whatsoever, and the fact that the Government may have formulated, furnished, or in any way supplied the said drawings, specifications, or other data, is not to be regarded by implication or otherwise, or in any manner licensing the holder or any other person or corporation, or conveying any rights or permission to manufacture, use, or sell any patented invention that may in any way be related thereto.

Qualified users may obtain copies of this report from the Defense Documentation Center.

References to named commercial products in this report are not to be considered in any sense as an endorsement of the product by the United States Air Force or the Government.

This report has been reviewed by the Information Office (OI) and is releasable to the National Technical Information Service (NTIS). At NTIS, it will be available to the general public, including foreign nations.

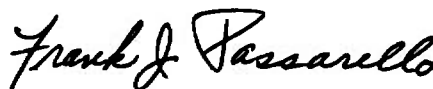
## APPROVAL STATEMENT

This technical report has been reviewed and is approved for publication.

FOR THE COMMANDER



JIMMY W. MULLINS  
Lt Colonel, USAF  
Chief Air Force Test Director, VKF  
Directorate of Test



FRANK J. PASSARELLO  
Colonel, USAF  
Director of Test

# UNCLASSIFIED

REPORT DOCUMENTATION PAGE		READ INSTRUCTIONS BEFORE COMPLETING FORM
1. REPORT NUMBER <b>AEDC-TR-75-91</b>	2. GOVT ACCESSION NO.	3. RECIPIENT'S CATALOG NUMBER
4. TITLE (and Subtitle) <b>VISCOUS EFFECTS ON THE STATIC STABILITY AND AXIAL-FORCE CHARACTERISTICS OF THE NASA SPACE SHUTTLE ORBITER AT MACH NUMBER 19</b>	5. TYPE OF REPORT & PERIOD COVERED <b>Final Report, February 10 - 17, 1975</b>	
	6. PERFORMING ORG. REPORT NUMBER	
7. AUTHOR(s) <b>L. G. Siler, ARO, Inc.</b>	8. CONTRACT OR GRANT NUMBER(s)	
9. PERFORMING ORGANIZATION NAME AND ADDRESS <b>Arnold Engineering Development Center (XO) Air Force Systems Command Arnold Air Force Station, TN 37389</b>	10. PROGRAM ELEMENT, PROJECT, TASK AREA & WORK UNIT NUMBERS <b>Program Element 921E</b>	
11. CONTROLLING OFFICE NAME AND ADDRESS <b>NASA-JSC (EX33) Houston, TX 77058</b>	12. REPORT DATE <b>December 1975</b>	
	13. NUMBER OF PAGES <b>34</b>	
14. MONITORING AGENCY NAME & ADDRESS (if different from Controlling Office)	15. SECURITY CLASS. (of this report) <b>UNCLASSIFIED</b>	
	15a. DECLASSIFICATION/DOWNGRADING SCHEDULE <b>N/A</b>	
16. DISTRIBUTION STATEMENT (of this Report)  <b>Approved for public release; distribution unlimited.</b>		
17. DISTRIBUTION STATEMENT (of the abstract entered in Block 20, if different from Report)  <i>1 Shuttle vehicle - - Stability</i>		
18. SUPPLEMENTARY NOTES  <b>Available in DDC.</b>		
19. KEY WORDS (Continue on reverse side if necessary and identify by block number) <b>space shuttles                      static stability orbits vehicles hypersonic flow</b>		
20. ABSTRACT (Continue on reverse side if necessary and identify by block number) <b>An experimental program was conducted in the AEDC-VKF Hypervelocity Wind Tunnel (F) at a nominal Mach number of 19 to determine the static stability and axial-force characteristics of a 0.01-scale model of the NASA Space Shuttle Orbiter. The tests were conducted at an angle of attack of 30 deg at free-stream Reynolds numbers (based on model length) from <math>0.1 \times 10^6</math> to <math>0.4 \times 10^6</math>. The results are compared to previous AEDC data at Mach numbers 8, 10, and 16.</b>		

## UNCLASSIFIED

## PREFACE

The work reported herein was conducted by the Arnold Engineering Development Center (AEDC), Air Force Systems Command (AFSC), at the request of the National Aeronautics and Space Administration (NASA/JSC), for the Rockwell International Space Division, Downey, California, under Program Element 921E. The results of the test were obtained by ARO, Inc. (a subsidiary of Sverdrup & Parcel and Associates, Inc.), contract operator of AEDC, AFSC, Arnold Air Force Station, Tennessee, under ARO Project Number V41F-28A. The author of this report was L. G. Siler, ARO, Inc. The data analysis was completed on March 19, 1975, and the manuscript (ARO Control No. ARO-VKF-TR-75-54) was submitted for publication on May 8, 1975.

## CONTENTS

	<u>Page</u>
1.0 INTRODUCTION . . . . .	5
2.0 APPARATUS	
2.1 Tunnel and Nozzle Description . . . . .	5
2.2 Model Description . . . . .	6
2.3 Instrumentation . . . . .	7
3.0 PROCEDURE	
3.1 Test Procedures . . . . .	8
3.2 Test Conditions . . . . .	8
3.3 Data Acquisition . . . . .	9
3.4 Data Reduction . . . . .	9
3.5 Data Precision . . . . .	10
4.0 RESULTS AND DISCUSSION . . . . .	11
5.0 CONCLUSIONS . . . . .	13
REFERENCES . . . . .	13

## ILLUSTRATIONS

### Figure

1. AEDC-VKF Tunnel F Plant . . . . .	15
2. Tunnel F Family of Contoured Nozzles . . . . .	16
3. NASA/RI 0.010-Scale Orbiter Model (51-0) . . . . .	17
4. Sketch Illustrating 0.010-Scale Orbiter Model (51-0) Details . . . . .	18
5. Sketch of Orbiter Model Installation in the Tunnel F 108-in. Test Section . . . . .	19
6. Typical Timewise Variation of Tunnel Conditions and Model Data . . . . .	20
7. Variation of Static Stability Coefficients with $\bar{V}_\infty$ , $\delta_e = 0$ , $\delta_{BF} = 0$ , $\alpha = 30$ deg . . . . .	21
8. Variation of Lift and Drag Coefficients with $\bar{V}_\infty$ , $\delta_e = 0$ , $\delta_{BF} = 0$ , $\alpha = 30$ deg . . . . .	22
9. Variation of Static Stability Coefficients with $\bar{V}_\infty$ , $\delta_e = 15$ deg, $\delta_{BF} = 16.3$ deg, $\alpha = 30$ deg . . . . .	23
10. Variation of Lift and Drag Coefficients with $\bar{V}_\infty$ , $\delta_e = 15$ deg, $\delta_{BF} = 16.3$ deg, $\alpha = 30$ deg . . . . .	24
11. Comparison of Static Stability Coefficients versus $\bar{V}_\infty$ for $\delta_e = 0$ , $\delta_{BF} = 0$ , $\delta_e = 15$ deg, and $\delta_{BF} = 16.3$ deg at $\alpha = 30$ deg . . . . .	25
12. $C_N$ versus $C_m$ for $\bar{V}_\infty = 0.03$ at $\alpha = 30$ deg . . . . .	26

**TABLES**

1. Test Summary – Test OA160 . . . . .	27
2. 0.010-Scale Orbiter Reference Dimensions . . . . .	27
3. Summary of Tunnel Conditions . . . . .	28
4. Summary of Aerodynamic Coefficients . . . . .	29
 NOMENCLATURE . . . . .	 30

## 1.0 INTRODUCTION

The National Aeronautics and Space Administration/Rockwell International (NASA/RI) Orbiter Force Test (OA160) was a program to verify the hypersonic stability and control characteristics of the 0.010-scale model (51-0) of a modified Vehicle 4 Orbiter configuration. Data were obtained at an angle of attack of 30 deg at zero sideslip angle for three different control surface deflection angles to determine trim capability and control surface effectiveness. The body was equipped with positionable elevons and body flap with a fixed speed brake and rudder. The testing was done at a nominal Mach number of 19 and at Reynolds numbers, based on free-stream conditions and model length, from approximately  $0.1 \times 10^6$  to  $0.4 \times 10^6$ . The data are compared to previous AEDC Orbiter data obtained at Mach numbers 8, 10, and 16.

## 2.0 APPARATUS

### 2.1 TUNNEL AND NOZZLE DESCRIPTION

The von Kármán Gas Dynamics Facility (VKF) Hypervelocity Wind Tunnel (F) (Fig. 1) is an arc-driven wind tunnel of the hotshot type (Refs. 1 and 2) and is capable of providing Mach numbers from about 7.5 to 20 over a Reynolds number per foot range from  $0.05 \times 10^6$  to  $70 \times 10^6$ . Tests are conducted in the 108-in.-diam test section ( $M_\infty = 14$  to 20) using a 4-deg half-angle conical nozzle. The range of Mach numbers is obtained by using various throat diameters. Tests are conducted in the 54-in.-diam test section ( $M_\infty = 8$  to 16) utilizing contoured nozzles as shown in Fig. 2. The  $M_\infty = 8, 12,$  and  $16^*$  contoured nozzles have 25-, 40-, and 48-in. exit diameters, respectively, which connect to the 54-in.-diam test station and provide a free-jet exhaust. The gas for aerodynamic and aerothermodynamic testing is nitrogen. Air is used for combustion tests. The test gas is confined in either a 1.0-ft<sup>3</sup>, a 2.5-ft<sup>3</sup>, or a 4.0-ft<sup>3</sup> arc chamber, where it is heated and compressed by an electric arc discharge. The increase in pressure results in a diaphragm rupture with the subsequent flow expansion through the nozzle. Test durations are typically from 50 to 200 msec. Shadowgraph and schlieren coverage are available at both test sections.

This test was conducted in the 108-in.-diam test section of the conical nozzle at  $M_\infty \approx 19$  with nitrogen as the gas. The 1.0-ft<sup>3</sup> volume arc chamber was used, and useful test times up to approximately 50 msec were obtained. Because of the relatively short test times, the model wall temperature remained essentially invariant from the initial value of approximately 540°R; thus  $T_w/T_o \approx 0.12$  and approximates the condition of practical interest for reentry vehicles.

---

\*The  $M_\infty = 16$  contoured nozzle is scheduled to become operational in October 1975.

## 2.2 MODEL DESCRIPTION

The model was a 0.010-scale model (51-0) of a modified NASA Vehicle 4 Orbiter. The full-scale vehicle has a body length of 1290.3 in. and a wingspan of 936.68 in., which corresponds to a model reference length and wingspan of 12.903 and 9.367 in., respectively. A photograph of the orbiter model is presented in Fig. 3. A sketch of the model indicating the general arrangement and pertinent reference stations and dimensions is shown in Fig. 4.

The model was designed and fabricated prior to the first tunnel F test series (OA81) by AEDC/VKF with the outside contours and overall dimensions traced from a master model provided by Rockwell International (RI), Huntsville, Alabama. The master model was fabricated in conformance with the line drawings as follows:

Nose	VL70-000143A
Mid-body and wing	VL70-000200
Aft body	VL70-000145
Vertical tail	VL70-000146A

The model was constructed of magnesium with all components hollowed or milled out where possible to reduce the overall weight. The upper surfaces of the wings were milled out and filled with foam with an epoxy coating. The model weighed approximately 1.8 lbm. Slight modifications to the outside contours of this model were made under the direction of RI, prior to the present test series (OA160) and according to the revised model dimensional data dated April 24, 1974.

The wings were equipped with positionable elevons with deflection angles obtained by exchanging angle plates machined to the desired angles. The elevon deflection angles used were  $\delta_e = -40, 0, \text{ and } 15$  deg with the extremes representing the limits of elevon travel for this configuration. Both the right and left elevons were split approximately midway of each span to represent the full-scale vehicle where aileron effects are desired; however, all elevon surfaces for this test were deployed at the same deflection angle for any given run. The elevon slits shown in Fig. 4 are not shown in Fig. 3 since they were added after the model was installed in the tunnel. A positionable body flap was provided by interchanging separate flaps machined to the proper deflection angles. Body flap angles used were  $\delta_{BF} = -11.7, 0, \text{ and } 16.3$  deg. The vertical stabilizer component had a fixed rudder and speed brake. Interchangeable stabilizers were available with speed brake deflection angles ( $\delta_{SB}$ ) of 0 and 55 deg. However, only the stabilizer with  $\delta_{SB} = 0$  was used during this test series. The vertical stabilizer shown in Fig. 3 with the speed brake deflection angle of 55 deg was not tested.

The NASA/Rockwell Orbiter model installation in Tunnel F is illustrated in Fig. 5.

### 2.3 INSTRUMENTATION

The aerodynamic forces were measured with a six-component force balance developed by AEDC/VKF for use in hotshot-type tunnels (Refs. 3 and 4). The balance load cells were instrumented with semiconductor strain gages, and semiconductor accelerometers provided compensation for model inertial loads that result from vibrations of the model and its support hardware. Tunnel F balances are now operated with constant current excitation. This type of excitation in combination with the characteristics of the semiconductor strain gages makes possible a compensation of the balance bridges so that the sensitivities are not affected significantly by changes in temperature. The result is an improvement in calibration accuracy and stability.

The balance used during the test series was calibrated before and after its use in the tunnel. The following uncertainties represent residuals which are differences between combined axial- and normal-force loads applied statically in the calibration laboratory and the corresponding values calculated from the data reduction equations. The applied range of static loading closely approximated the aerodynamic test loads:

<u>Balance Component</u>	<u>Range of Static Load Applied, lb</u>	<u>Measurement Uncertainty, Absolute, lb</u>
$F_{A_t}$	0.5 - 3	$\pm 0.013$
$F_{N_F}$	0.8 - 12	$\pm 0.008$
$F_{N_A}$	1.2 - 18	$\pm 0.009$

Base pressure measurements were made using variable reluctance differential pressure transducers with a range from 0.001 to 0.1 psia. The gages were mounted on the sting with the gage orifice positioned approximately 1/16 in. downstream of the model base.

Two gages were mounted in the nose of the orbiter model ("T" arrangement on a single orifice) to measure model  $p'_o$ . The gages used were 15-psid strain-gage pressure transducers calibrated at the specific pressure level occurring during each test condition.

The arc chamber pressure, test section pitot pressure, and test section heat-transfer rates on a hemisphere-cylinder probe were monitored to determine tunnel flow conditions. The arc chamber reservoir pressure was measured using two strain-gage transducers, each having full-scale calibrated ranges of 5, 10, and 25 thousand psia. The test section pitot pressures were measured using 2.0-psid strain-gage transducers calibrated for the range of

the specific test condition. The stagnation heat-transfer rates used in determining the tunnel flow conditions were inferred from measurements made on the cylindrical section of a 1.0-in.-diam hemisphere-cylinder probe using resistance thermometer slug calorimeters. Slug calorimeters have a thin-film platinum resistance thermometer to sense the temperature of an aluminum disk which is exposed to the heat flux to be measured. The calorimeters are optimized to measure a given range of heat transfer by appropriate selection of the aluminum disk thickness.

Detailed information about the force, heat-transfer, and pressure instrumentation may be found in Refs. 2, 3, and 4.

### 3.0 PROCEDURE

#### 3.1 TEST PROCEDURES

The test objective was to determine the static stability and axial-force characteristics of the modified Vehicle 4 Orbiter configuration at Mach number 19 over a Reynolds number ( $Re_{\infty, \rho}$ ) range from  $0.1 \times 10^6$  to  $0.4 \times 10^6$  at an angle of attack of 30 deg. The elevon and body flap deflection angles were varied for determination of control effectiveness. The primary model configuration tested had all the control surfaces at zero deflection angle, including the speed brake, which was fixed at zero deflection throughout the test series.

A series of runs was made with both the elevons and body flap positioned at their positive deflection limits ( $\delta_e = 15$  deg,  $\delta_{BF} = 16.3$  deg). This series was tested primarily to verify the trim capability of the configuration at these control surface settings. Both these series of runs were made at the two Reynolds number conditions.

Additional runs were made during both test series with the model inverted ( $\phi = 180$  deg) and the model nose pitched toward the bottom of the tunnel. These runs were made to assist in determining the corrections to apply to the data for small tunnel flow nonuniformities. The location of the model in the test section for both positions is shown in Fig. 5. One run was made with both the elevons and the body flap positioned at their negative deflection limits ( $\delta_e = -40$  deg,  $\delta_{BF} = -11.7$  deg). A complete test summary indicating the primary variables during the test is given in Table 1. Table 2 lists the 0.10-scale Orbiter reference dimensions.

#### 3.2 TEST CONDITIONS

The method of determining the tunnel flow conditions is briefly summarized as follows: instantaneous values of reservoir pressure ( $p_o$ ) and free-stream pitot pressure ( $p'_o$ )

are measured and an instantaneous value of the stagnation heat-transfer rate ( $\dot{q}_o$ ) is inferred from a direct measurement of a shoulder heat rate on a 1.0-in.-diam hemisphere cylinder heat probe. Total enthalpy ( $H_o$ ) is calculated from  $p_o'$ ,  $\dot{q}_o$ , and the heat probe radius, using Fay-Riddell theory, Ref. 5. The value of  $H_o$  determined in this manner and the measured value of reservoir pressure are then used to determine corresponding values of reservoir temperature, density, and entropy from tabulated thermodynamic data for nitrogen (Ref. 6). The reservoir conditions, the measured value of  $p_o'$ , and the assumption of isentropic flow in the nozzle are then used to compute the free-stream conditions. The basic procedure followed in this computation is given in Refs. 7 and 8.

A summary of the reservoir and free-stream conditions is given in Table 3.

### 3.3 DATA ACQUISITION

All data were recorded on a 70-channel digital system capable of scanning all channels in 1 msec and storing up to 150 scans of data. Basic data reduction was done off-line on a digital computer.

As a backup to the digital system, as well as to provide a quick look at the data results, the output of each data channel was recorded on an oscillograph. Figure 6 represents examples of the analog traces for the tunnel monitor information ( $p_o$ ,  $p_o'$ ,  $p_B$ , and  $\dot{q}_o$ ) and compensated force data traces ( $F_{NF}$ ,  $F_{NA}$ , and  $F_A$ ). Calculated values of free-stream unit Reynolds number ( $Re_\infty/ft$ ) and Mach number ( $M_\infty$ ) are shown to illustrate timewise variations of test conditions. Note that there is a 55-msec delay from the initial pressure rise to the start of the useful run; this delay is attributable to the nozzle starting process and to the time required for the free-stream temperature to equal or exceed the theoretical saturation temperature of nitrogen.

### 3.4 DATA REDUCTION

The model nose  $p_o'$  measurements were used in the calculations for determining the free-stream test section conditions. The force data are normalized by the dynamic pressure, which is thus dependent on the measured model nose pressure.

Since the Tunnel F nozzle providing flow in the 108-in.-diam test section is conical, source flow effects are present. Adjustments were made to the data to correct for these following the discussion of source flow corrections in Ref. 2. Corrections were determined assuming the pressure coefficient at any station on the "flat-bottomed" orbiter vehicle could be described by the Newtonian expression as a function of angle of attack and source flow angle. The calculated corrections indicated a 0.22-percent rearward shift in  $X_{cpN}/\ell$  was required to correct for source flow. The normal- and axial-force coefficient

corrections were less than 1 percent and were considered insignificant when compared to the measurement uncertainties; thus no corrections to  $C_N$  and  $C_A$  were made.

Additional corrections to  $X_{cpN}/\ell$  and  $C_N$  were applied to compensate for flow nonuniformities and a source flow angle resulting from the location of the model in the test section. These corrections were determined from a comparison of the aerodynamic data obtained with the model in the normal upright mode and data obtained with the model and balance inverted ( $\phi = 180$  deg) and pitched toward the bottom of the tunnel. The model was tested in the top half of the tunnel with the trailing edge of the body flap approximately 1 in. above the tunnel centerline for the upright position and the nose approximately 1 in. above the tunnel centerline for the inverted position. The accompanying source flow angle and the flow nonuniformities were accounted for by averaging the  $X_{cpN}/\ell$  and  $C_N$  coefficients for the upright and inverted runs for each of the respective configurations at each of the Reynolds number conditions. The resulting corrections were a maximum 2-percent change in  $C_N$  and a maximum 0.4-percent shift in  $X_{cpN}/\ell$ . The pitching moments were recomputed to reflect the corrections to the center of pressure,  $X_{cpN}/\ell$ , and the normal-force coefficient,  $C_N$ . A summary of the force coefficients is given in Table 4.

### 3.5 DATA PRECISION

The uncertainties in the monitor probe measurements ( $p'_o$  and  $\dot{q}_o$ ) and arc chamber measurements ( $p_o$ ) considering both static load calibrations, system errors, and data repeatability, are estimated to be  $\pm 4$ ,  $\pm 7$ , and  $\pm 5$  percent, respectively. The  $p'_o$  and  $p_o$  uncertainties are based on the average of two measurements and the uncertainty of  $\dot{q}_o$  on the inferred value from the average of two probe shoulder measurements. These values were used to estimate uncertainties in the tunnel flow parameters using the Taylor series method of error propagation. Representative parameters are given below.

Uncertainty ( $\pm$ ), percent

<u><math>M_\infty</math></u>	<u><math>Re_\infty \ell</math></u>	<u><math>T_\infty</math></u>	<u><math>p_\infty</math></u>	<u><math>q_\infty</math></u>	<u><math>\dot{q}_o</math></u>	<u><math>p_o</math></u>	<u><math>p'_o</math></u>
1.5	12	7	6	4	7	5	4

The uncertainties in the calculated force data were estimated by using the Taylor series method of error propagation to combine the uncertainties in each measurement occurring in the calculations. In general, it is estimated that for nominal loads the uncertainty in the force measurements is  $\pm 6$  percent for each balance component. This uncertainty includes calibration linearity and repeatability, instrumentation system error, and errors introduced by dynamic effects resulting from the impulsive operating nature of the facility. The uncertainty of  $\pm 6$  percent of each balance component measurement

combined with a  $\pm 4$ -percent uncertainty in the dynamic pressure gives an uncertainty in the force coefficient,  $C_N$ , of  $\pm 6$  percent for the load distribution observed during this test. An uncertainty of  $\pm 6$  percent of the measured axial force combined with a  $\pm 4$ -percent uncertainty in the dynamic pressure gives an uncertainty in  $C_A$  of  $\pm 7$  percent.

The absolute uncertainties in pitching-moment and center-of-pressure location were determined using the Taylor series method of error propagation. The uncertainties are primarily a function of the load distribution of the normal-force component measurements with the axial-force component being a minor influence.

<u>Absolute Uncertainties</u>	
<u><math>C_m</math></u>	<u><math>X_{cpN}/\ell</math></u>
$\pm 0.0163$	$\pm 0.0076$

The above-quoted percent uncertainties in  $C_N$  and  $C_A$  and the absolute uncertainties in  $C_m$  and  $X_{cpN}/\ell$  apply to all the tabulated data presented in this report. It should be noted that these uncertainties apply to each data point and are not necessarily indicative of the overall uncertainty of a force coefficient when the data are plotted versus some parameter, e.g.,  $\bar{V}_\infty$ , and a fairing is made through all the data. The following near-minimum load uncertainties were determined using the balance residuals as discussed in Section 2.3 in conjunction with the Taylor series method of error propagation and are included here to indicate the lower resolution limits of the balance.

<u>Near-Minimum Load Uncertainties</u>				
Nominal <u><math>Re_{\infty, \ell}</math></u>	Nominal <u><math>q_\infty</math></u>	<u><math>C_A</math></u>	<u><math>C_N</math></u>	<u><math>C_m</math></u>
0.35	0.50	0.00067	0.00062	0.00020
0.12	0.17	0.00197	0.00183	0.00059

However, for this report the uncertainty levels to be applied to the data are not the above near-minimum load uncertainties but rather the previously mentioned percent  $C_N$  and  $C_A$  uncertainties of  $\pm 6$  and  $\pm 7$  percent, respectively, and the absolute uncertainty of  $\pm 0.0163$  for  $C_m$  and  $\pm 0.0076$  for  $X_{cpN}/\ell$ . The model attitude was set prior to each run; the pitch angle is estimated to be accurate within  $\pm 0.10$  deg. The estimated uncertainties for the model base pressure measurements are  $\pm 10$  percent.

#### 4.0 RESULTS AND DISCUSSION

All of the data taken during this test series were at an approximate Mach number of 19 and at an angle of attack of 30 deg. Analysis of these data over the Reynolds

number range tested and comparisons with previous AEDC data obtained at Mach numbers of 8, 10, and 16 show a definite dependence of the aerodynamic characteristics of the Orbiter configuration upon the visous parameter  $\bar{V}_\infty$  (hence altitude and velocity). A detailed discussion of the  $\bar{V}_\infty$  parameter can be found in Ref. 9

Variations of the static stability coefficients with  $\bar{V}_\infty$  are shown in Fig. 7 for the Orbiter configuration with the elevon and body flap control surfaces at zero deflection. Data are included in this figure and in subsequent figures from previous unpublished AEDC Orbiter test results for comparison. All data fairings except  $C_N$  shown in these figures are linear least-squares fits of the Mach number 10 through 19 data only. It is seen that the axial force is very sensitive to  $\bar{V}_\infty$ , as a factor of 3 increase in  $C_A$  is noted between the Mach number 10 test condition and the Mach number 19 low Reynolds number data. The normal-force coefficient is essentially invariant with  $\bar{V}_\infty$  within the data scatter. However, there is a definite rearward shift in  $X_{cpN}/\ell$ , which results in a more negative pitching moment with increasing  $\bar{V}_\infty$ .

Figure 8 indicates the variation of the lift and drag coefficients with  $\bar{V}_\infty$  at an angle of attack of 30 deg for the same configuration. Approximately a 30-percent reduction in the lift-to-drag ratio is shown for the increase in  $\bar{V}_\infty$ .

Similar results are shown in Figs. 9 and 10 for the configuration with the elevons and body flap at their extreme positive (into the wind) deflections. Again, in Fig. 9, a substantial increase in  $C_A$  is noted with increasing  $\bar{V}_\infty$ . The lift and drag coefficients in Fig. 10 show trends similar to that of the basic configuration (all control surface deflection angles at zero). However, the center-of-pressure location (Fig. 9) shifts forward with increasing  $\bar{V}_\infty$  with the pitching moment becoming less negative. This is the opposite trend to the zero flap deflection configuration (Fig. 7). This is illustrated clearly in Fig. 11, where the data fairings from Figs. 7 and 9 are shown. This difference in trend with  $\bar{V}_\infty$  is attributed to the  $\bar{V}_\infty$  effect on the separation which is probably occurring at the flap. In essence the separation is causing the flap to lose effectiveness as  $\bar{V}_\infty$  is increased, and this is overshadowing any rearward shift in  $(X_{cpN}/\ell)$  caused by increased shear effect.

Only one run was made on the Orbiter configuration with the elevons and body flap retracted out of the wind. The results of this run are indicated in a conventional plot of  $C_N$  versus  $C_m$  in Fig. 12, which includes data for all three elevon and body flap deflection angles. Data are shown for a constant  $\bar{V}_\infty$  of 0.03. The plot indicates the control effectiveness of the elevon-body flap settings at an angle of attack of 30 deg.

Under the conditions of concern during this test series, the similarity parameters of importance in extrapolating from wind tunnel to flight conditions include not only

geometric similarity, Mach numbers and Reynolds numbers, but also enthalpy ratio ( $H_w/H_\delta$ ), Prandtl number, normalized velocity ( $V_\delta^2/H_\delta$ ), and the exponent in the viscosity-temperature law ( $\mu = T^\omega$ ), cf. Ref. 10, pp. 215-218. Thus care is demanded in using perfect-gas wind tunnel data such as are presented herein for purposes of predicting reentry of the full-scale vehicle.

## 5.0 CONCLUSIONS

Static force and moment measurements were made on a modified NASA Vehicle 4 Orbiter configuration at an angle of attack of 30 deg over a Reynolds number range from  $0.1 \times 10^6$  to  $0.4 \times 10^6$  ( $Re_{\infty, \rho}$ ).

An analysis of the data indicates that the orbiter static stability and axial-force characteristics are sensitive to the viscous parameter  $\nabla_\infty$  (and hence to altitude and velocity). Because of the similarity parameters of importance when extrapolating from wind tunnel to flight conditions, it is necessary to exercise care in using perfect-gas wind tunnel data such as are presented herein for purposes of predicting reentry of the full-scale vehicle.

## REFERENCES

1. Test Facilities Handbook (Tenth Edition). "von Kármán Gas Dynamics Facility, Vol. 3." Arnold Engineering Development Center, May 1974.
2. Pate, S. R. and Eaves, R. H., Jr. "Recent Advances in the Performance and Testing Capabilities of the AEDC-VKF Tunnel F (HOTSHOT) Hypersonic Facility. AIAA Paper No. 74-84, presented at the AIAA 12th Aerospace Sciences Meeting, Washington, D.C., January 30-February 1, 1974.
3. Ledford, R. L., Smotherman, W. E., and Kidd, C. T. "Recent Developments in Heat-Transfer-Rate, Pressure, and Force Measurements for Hotshot Tunnels." AEDC-TR-66-228 (AD645764), January 1967.
4. Bynum, D. S. "Instrumentation for the AEDC/VKF 100-in. Hotshot (Tunnel F)." AEDC-TR-66-209 (AD804567), January 1967.
5. Fay, J. A. and Riddell, F. R. "Theory of Stagnation Point Heat Transfer in Dissociated Air." Journal of Aeronautical Sciences, Vol. 25, No. 2, February 1958, pp. 73-85, 121.
6. Brahinsky, Herbert S. and Neel, Charles A. "Tables of Equilibrium Thermodynamic Properties of Nitrogen." Vols. I-IV, AEDC-TR-69-126 (AD693134, AD692712, AD692713, AD692172), August 1969.

7. Grabau, Martin, Smithson, H. K., Jr., and Little, W. J. "A Data Reduction Program for Hotshot Tunnels Based on the Fay-Riddell Heat-Transfer Rate Using Nitrogen at Stagnation Temperatures from 1500°K to 5000°K." AEDC-TR-64-50 (AD601070), June 1964.
8. Griffith, B. J. and Lewis, Clark H. "Laminar Heat Transfer to Spherically Blunted Cones at Hypersonic Conditions." AIAA Journal, Vol. 2, No. 3, March 1964, pp. 438-444.
9. Whitfield, Jack D. and Griffith, B. J. "Viscous Effects on Zero-Lift Drag of Slender Blunt Cones." AEDC-TR-63-35 (AD298278), March 1963, also AIAA Journal, Vol. 2, No. 10, October 1964, pp. 1714-1722.
10. Potter, J. Leith. "Low-Density Wind Tunnels." In Molecular Beams and Low-Density Gas Dynamics (P.P. Wegener, Ed.), Marcel Dekker, Inc., New York, 1974.

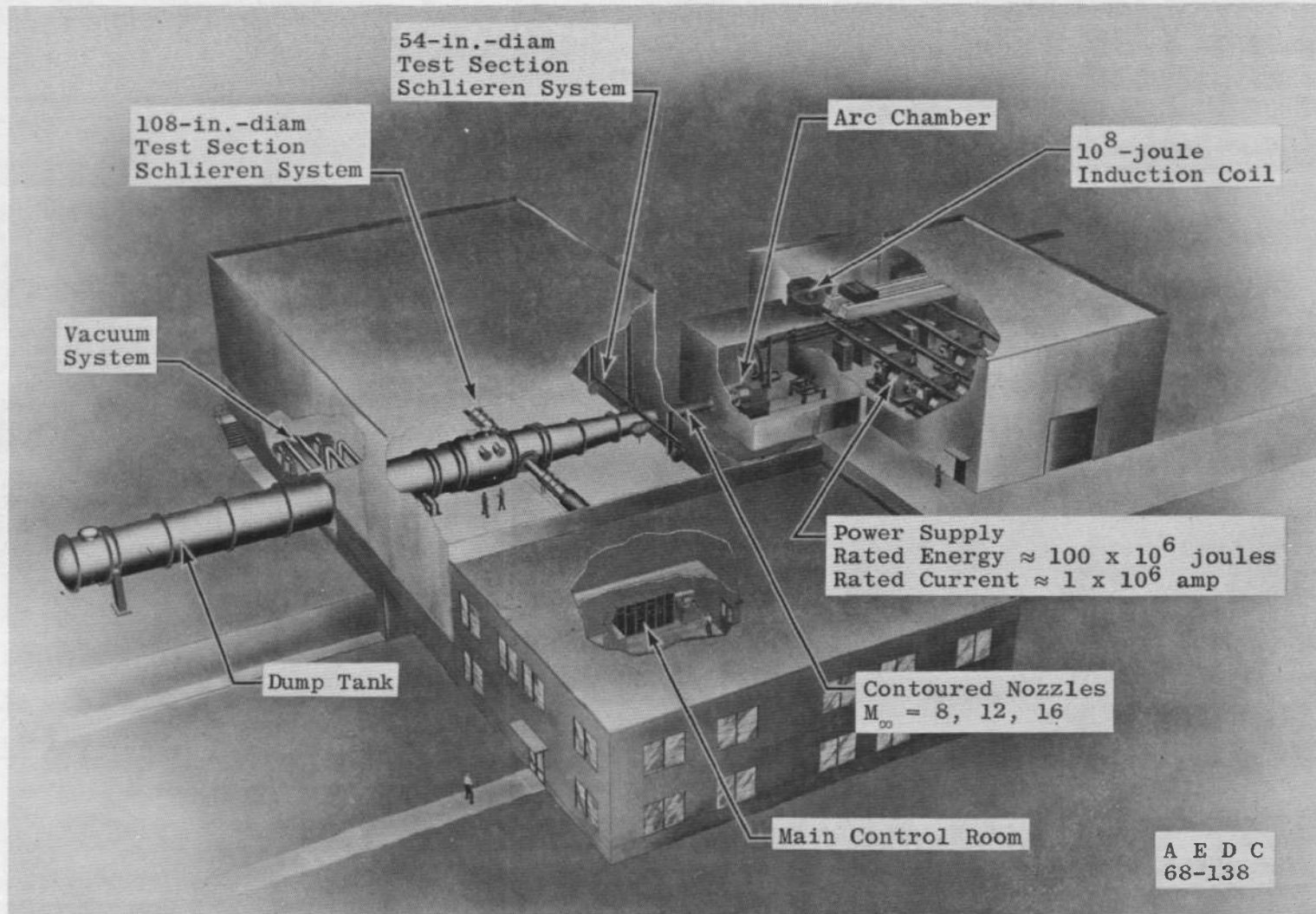


Figure 1. AEDC-VKF Tunnel F Plant.

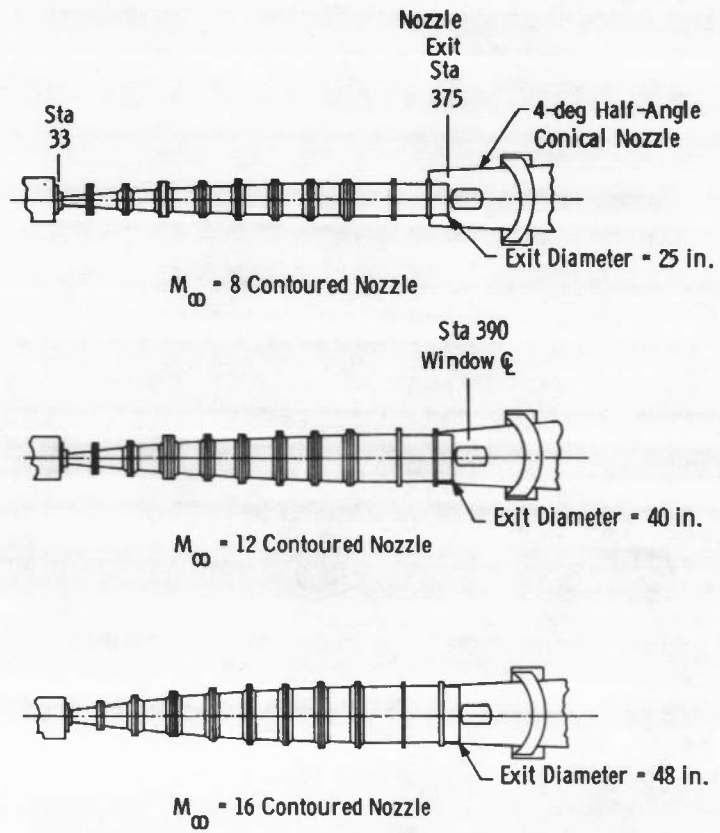
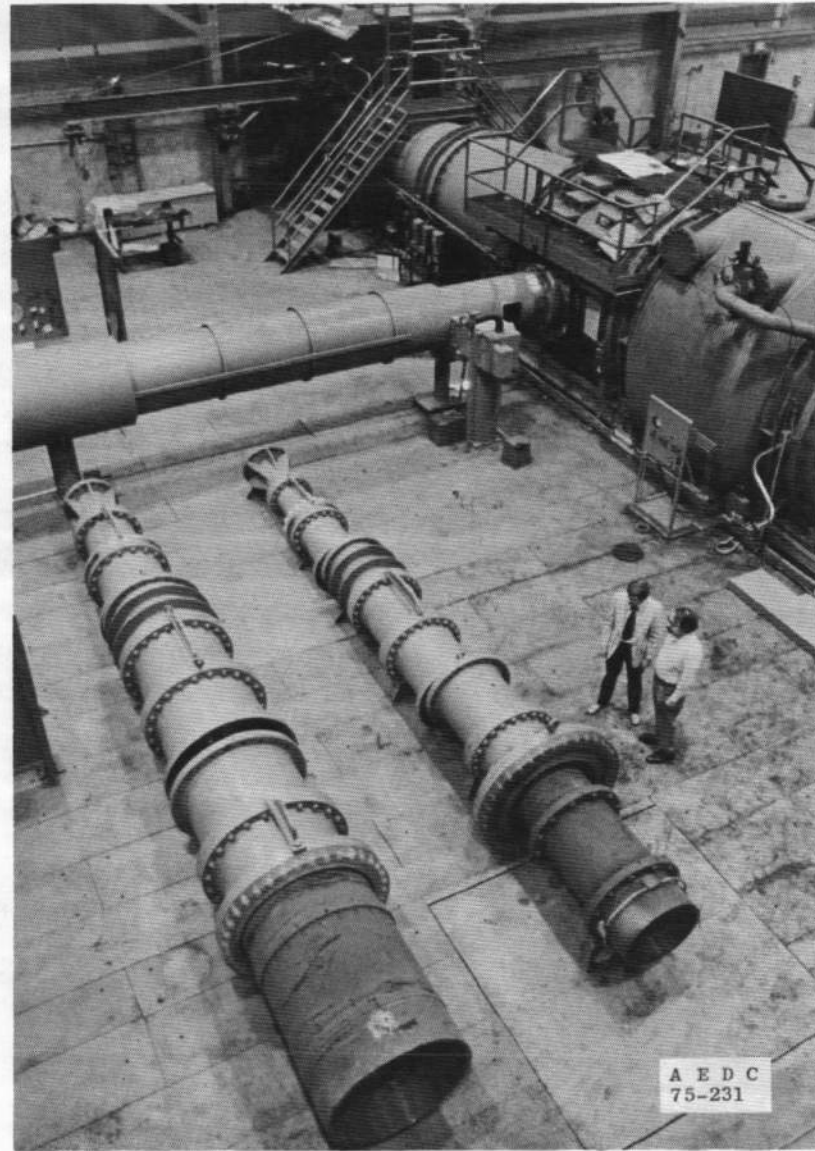


Figure 2. Tunnel F family of contoured nozzles.



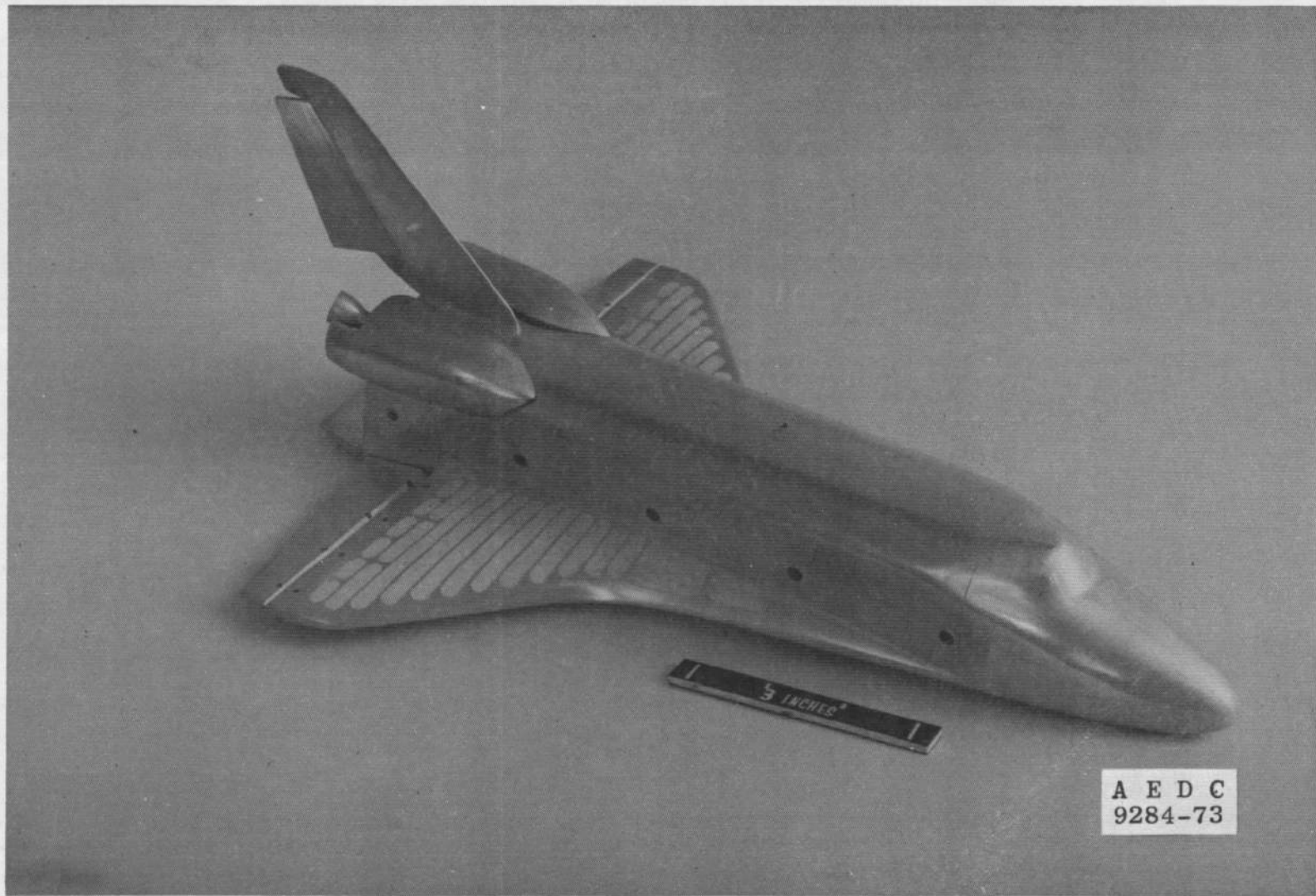


Figure 3. NASA/R1 0.010-scale Orbiter model (51-0).

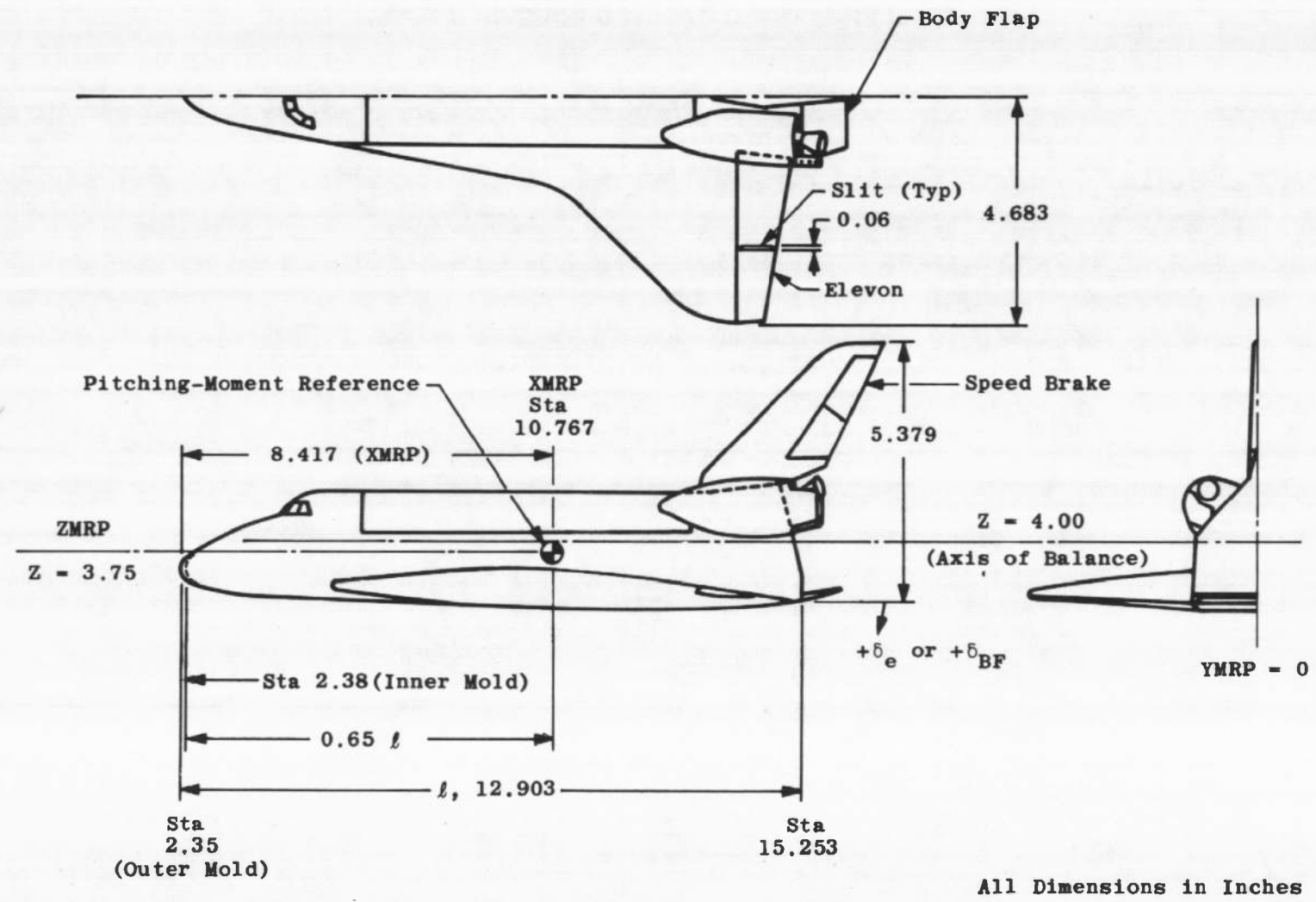


Figure 4. Sketch illustrating 0.010-scale Orbiter model (51-0) details.

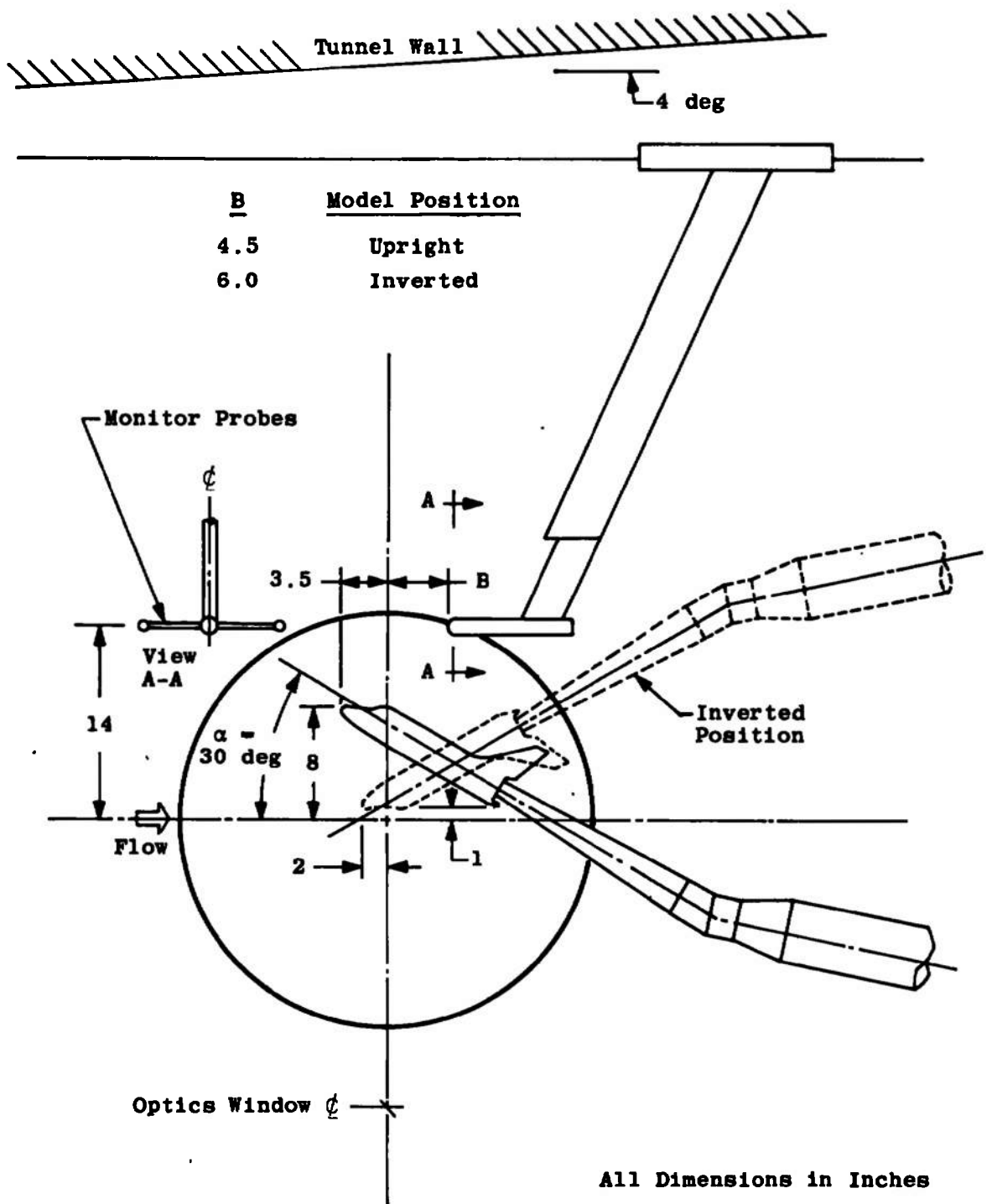


Figure 5. Sketch of Orbiter model installation in the Tunnel F 108-in. test section.

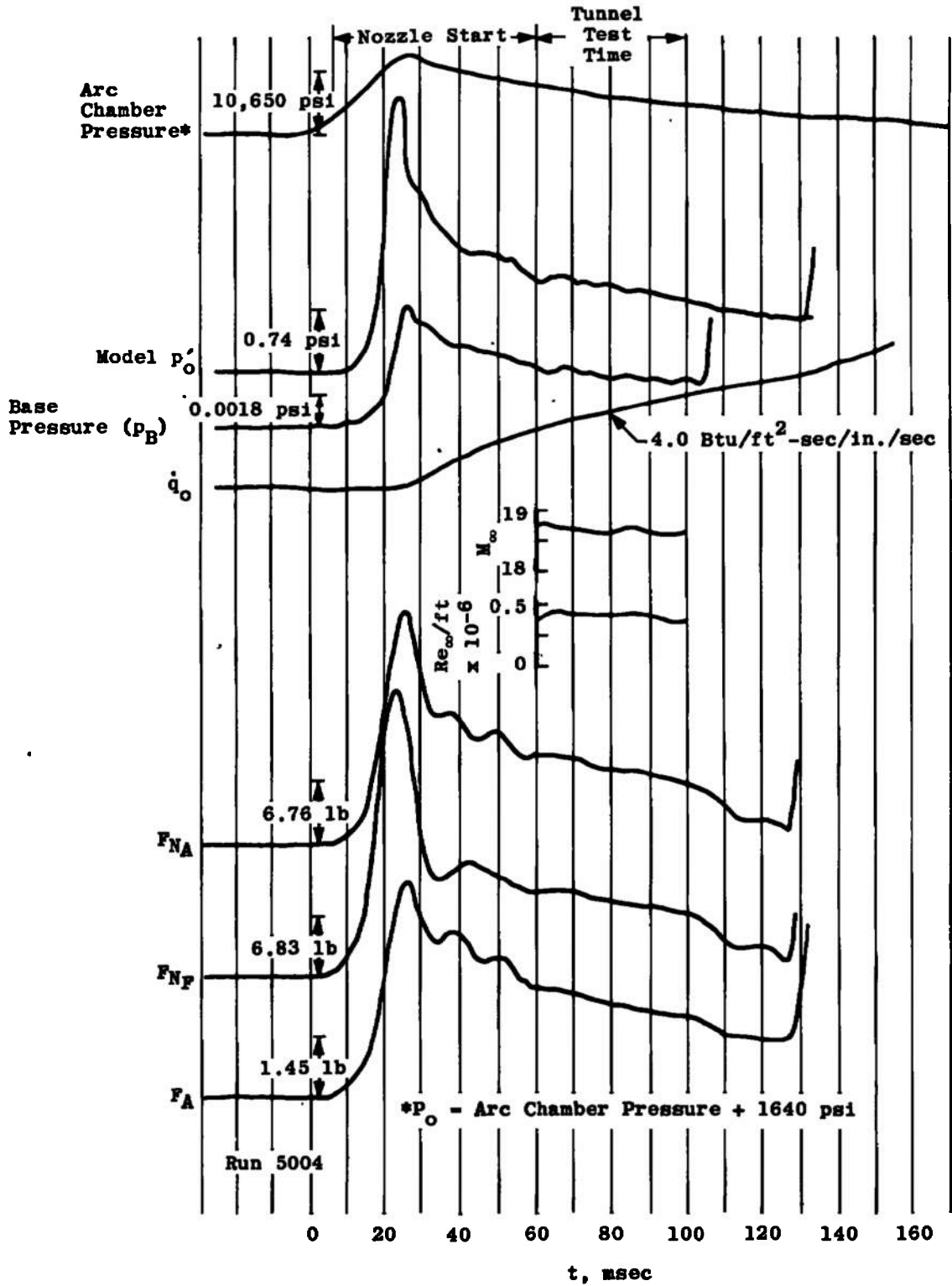


Figure 6. Typical timewise variation of tunnel conditions and model data.

Sym	Tunnel	$M_\infty$	$Re_{\infty, l}$ $\times 10^{-6}$	$\bar{\epsilon}_{SB}$	Test
▲	B	6.0	7.52	55	OA77
▼	B	8.0	5.65	55	OA77
◆	C	10.1	3.05	55	OA78
□	F	≈16	0.4 to 1.33	55	OA81
○	F	≈19	0.08 to 0.38	0	OA160 - Present Test

--- Data Fairing (Mach 10 through 19 Data Only)

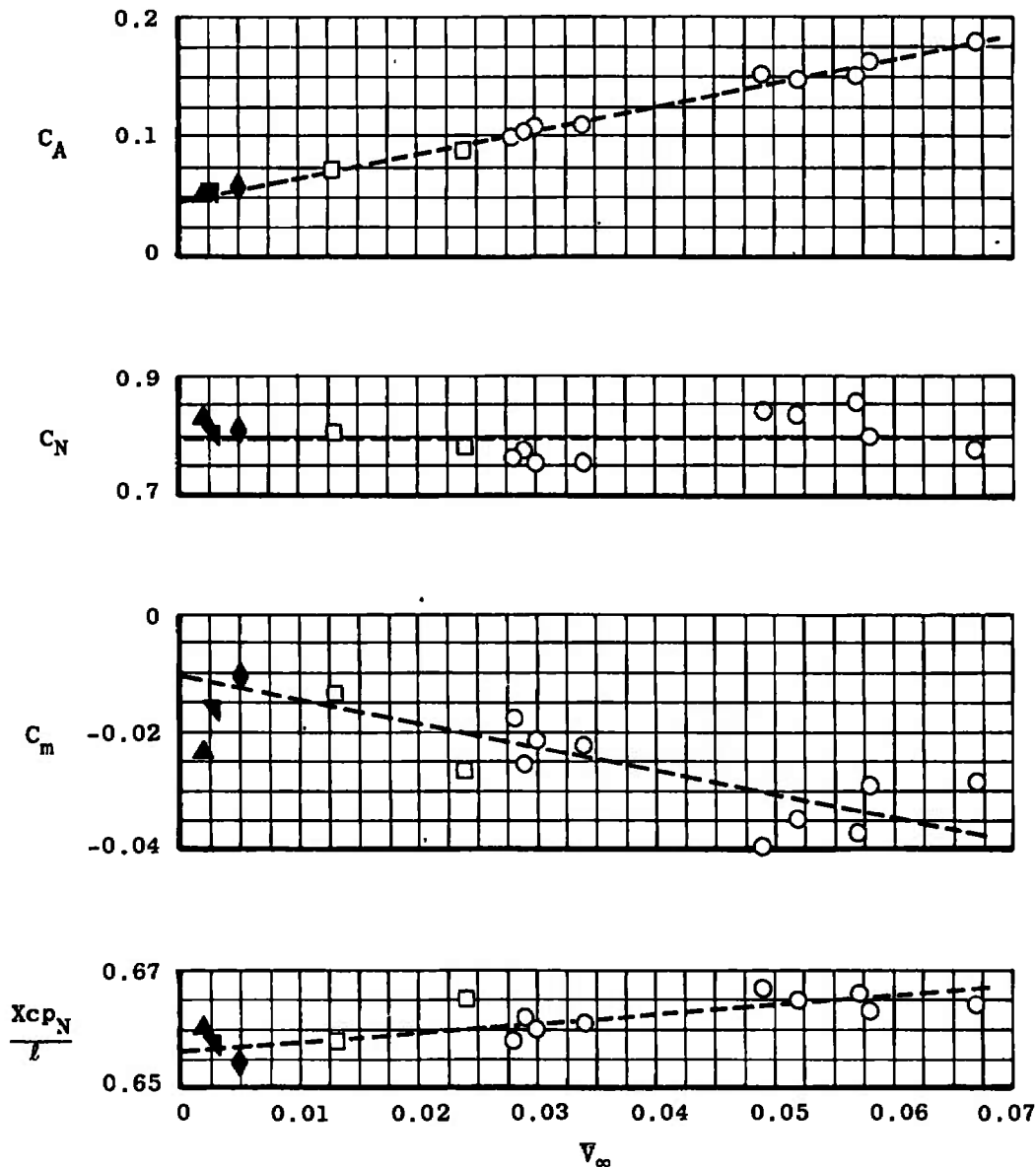


Figure 7. Variation of static stability coefficients with  $\bar{V}_\infty$ ,  
 $\delta_\theta = 0, \delta_{BF} = 0, \alpha = 30$  deg.

Sym	Tunnel	$M_\infty$	$Re_{\infty, l}$	$\delta_{SB}$	Test
			$\times 10^{-6}$		
▲	B	6.0	7.52	55	OA77
▼	B	8.0	5.65	55	OA77
◆	C	10.1	3.05	55	OA78
□	F	≈16	0.4 to 1.33	55	OA81
○	F	≈19	0.08 to 0.38	0	OA160 - Present Test

--- Data Fairing (Mach 10 through 19 Data Only)

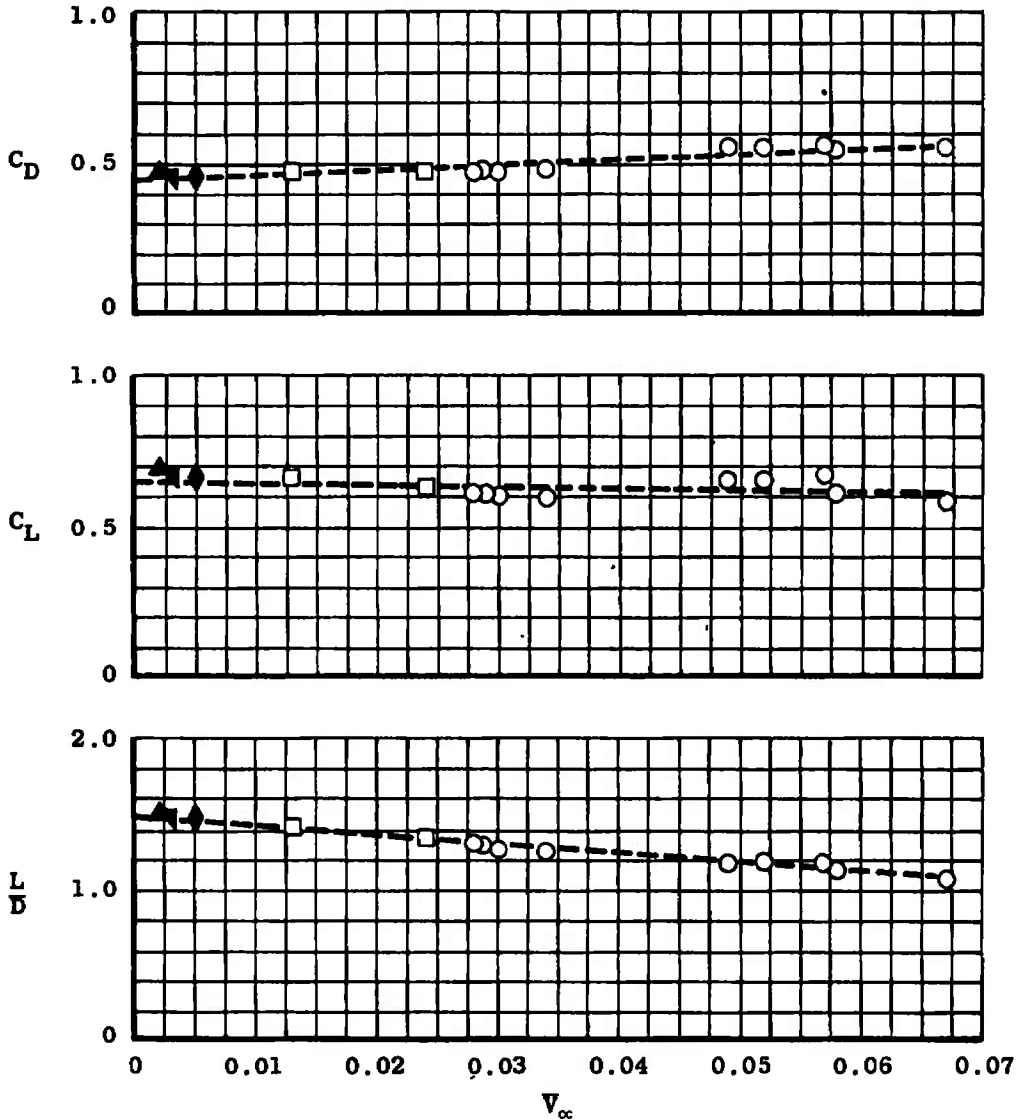


Figure 8. . Variation of lift and drag coefficients with  $\bar{V}_\infty$ ,  $\delta_e = 0$ ,  $\delta_{BF} = 0$ ,  $\alpha = 30$  deg.

Sym	Tunnel	$M_\infty$	$Re_{\infty, l}$ $\times 10^{-6}$	$^5SB$	Test
▲	B	6.0	7.53	55	OA77
▼	B	8.0	5.65	55	OA77
◆	C	10.1	3.05	55	OA78
□	F	16.3	0.98	55	OA81
○	F	≈19	0.11 to 0.30	0	OA160 - Present Test

--- Data Fairing (Mach 10 through 19 Data Only)

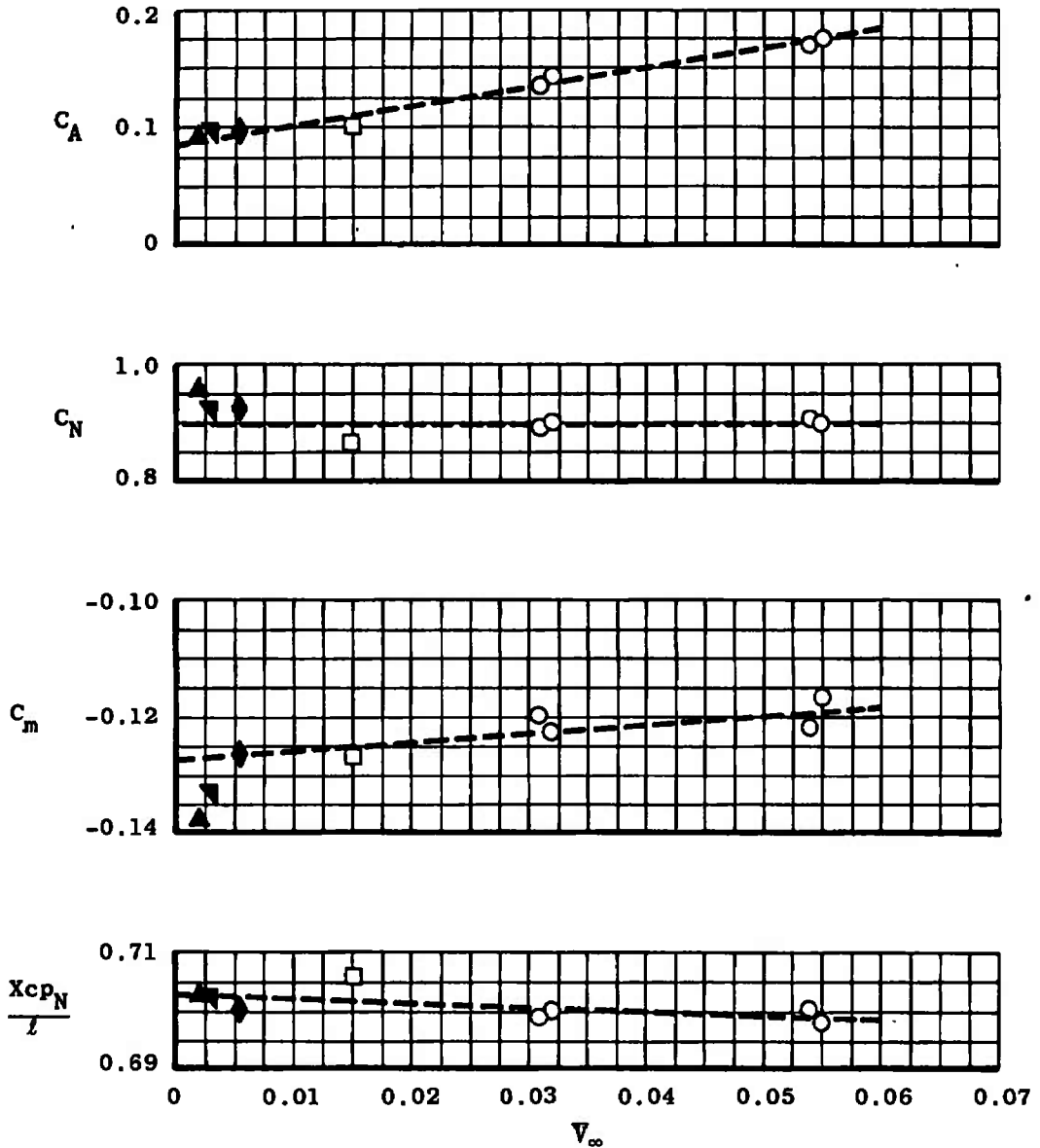


Figure 9. Variation of static stability coefficients with  $\bar{V}_\infty$ ,  
 $\delta_s = 15$  deg,  $\delta_{BF} = 16.3$  deg,  $\alpha = 30$  deg.

Sym	Tunnel	$M_\infty$	$Re_{\infty, l}$ $\times 10^{-6}$	$\delta_{SB}$	Test
▲	B	6.0	7.53	55	OA77
▼	B	8.0	5.65	55	OA77
◆	C	10.1	3.05	55	OA78
□	F	16.3	0.98	55	OAB1
○	F	≈19	0.11 to 0.30	0	OA160 - Present Test

— — — Data Fairing (Mach 10 through 19 Data Only)

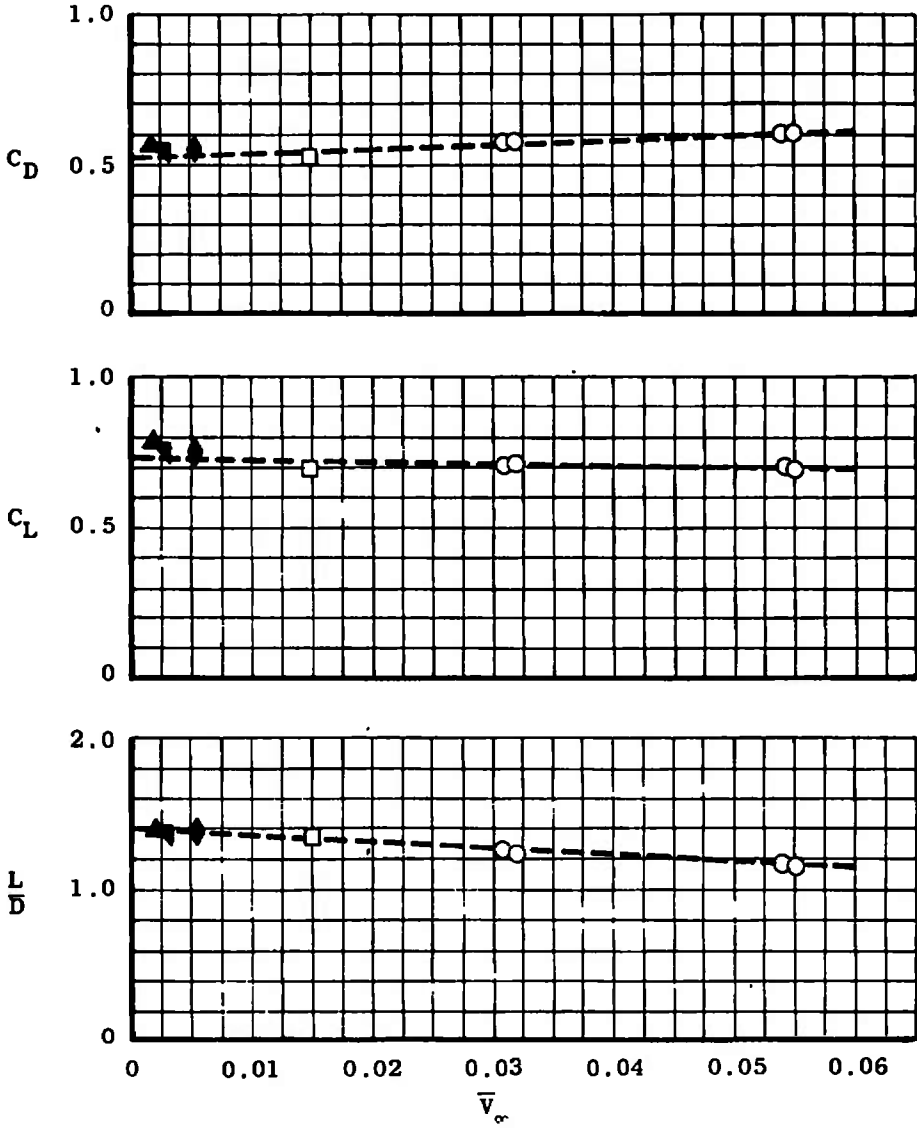


Figure 10. Variation of lift and drag coefficients with  $\bar{V}_\infty$ ,  $\delta_\theta = 15$  deg,  $\delta_{BF} = 16.3$  deg,  $\alpha = 30$  deg.

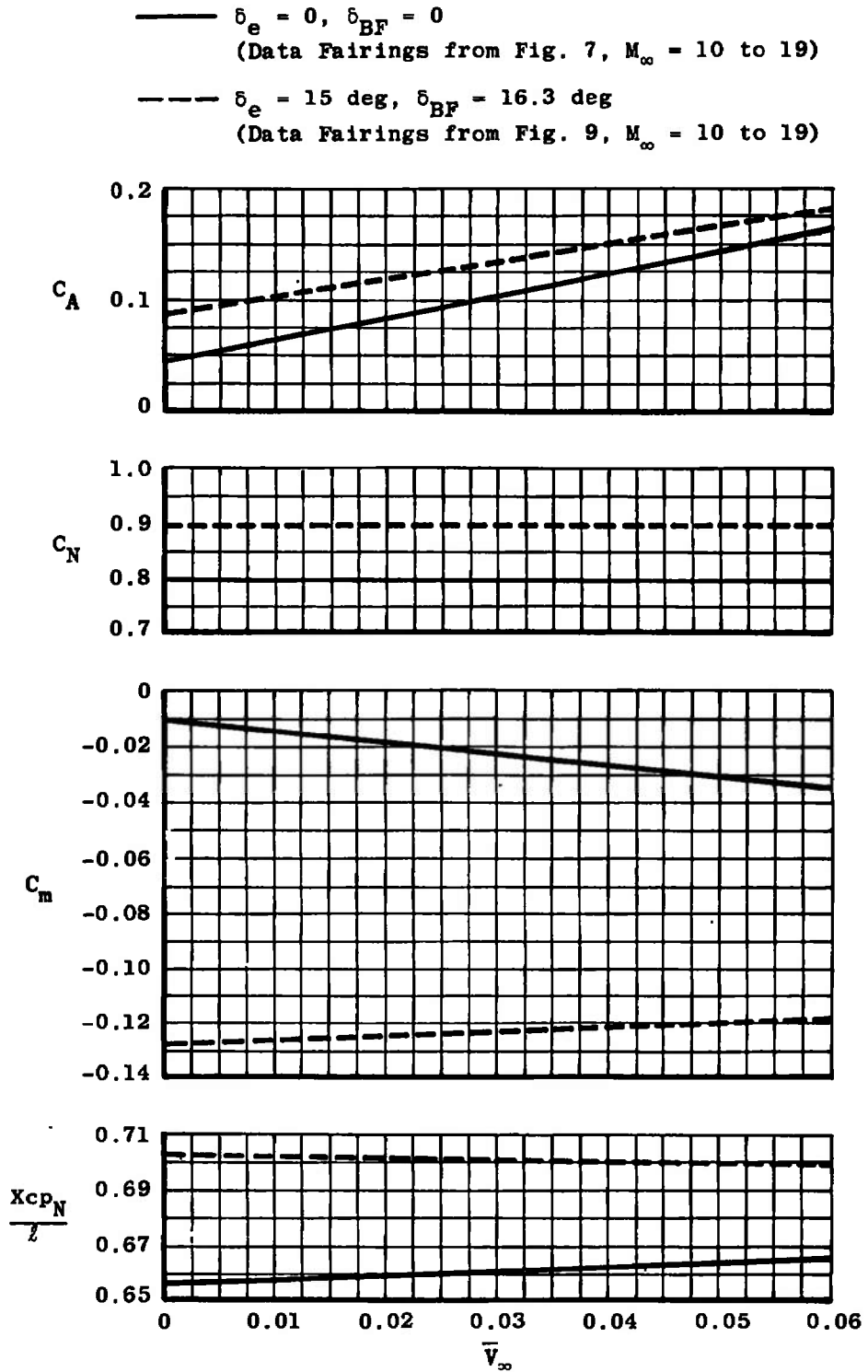


Figure 11. Comparison of static stability coefficients versus  $\bar{V}_\infty$  for  $\delta_e = 0$ ,  $\delta_{BF} = 0$ ,  $\delta_e = 15 \text{ deg}$ , and  $\delta_{BF} = 16.3 \text{ deg}$  at  $\alpha = 30 \text{ deg}$ .

<u>Sym</u>	<u>Tunnel</u>	$\frac{M_\infty}{}$	$\frac{\bar{V}_\infty}{}$	<u>Test</u>
○	F	19	0.03	OA160

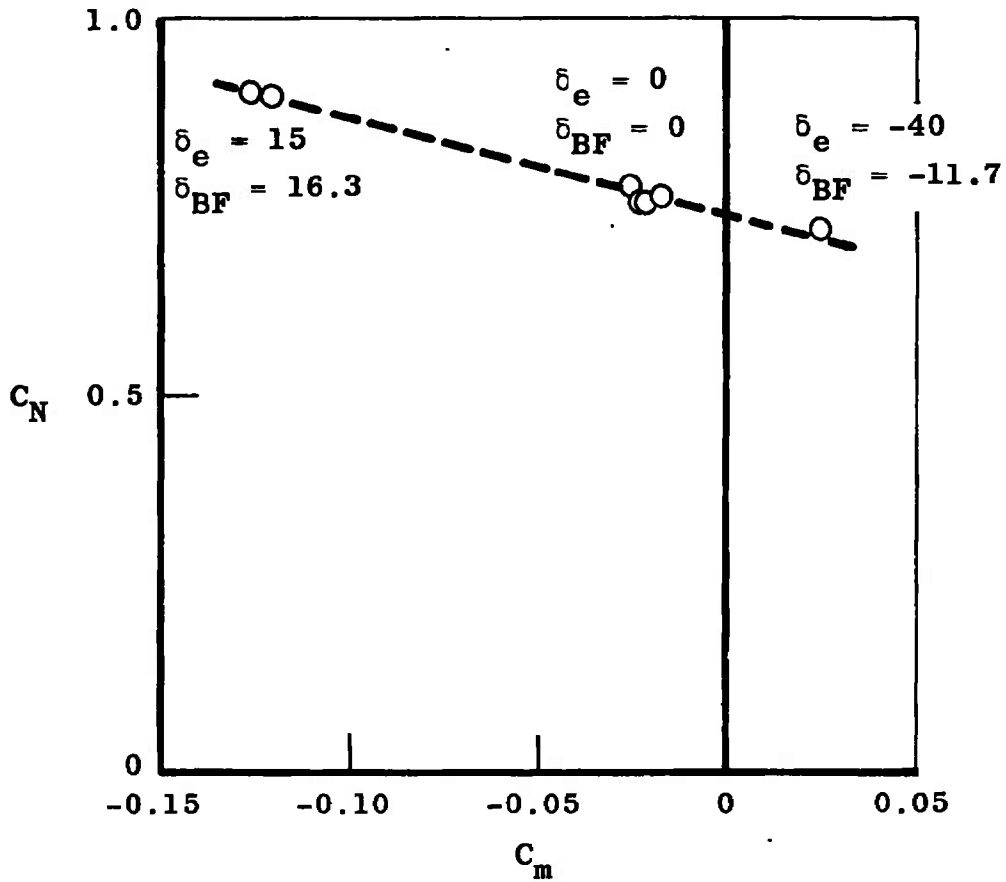


Figure 12.  $C_N$  versus  $C_m$  for  $\bar{V}_\infty = 0.03$  at  $\alpha = 30$  deg.

Table 1. Test Summary – Test OA160

<u>Tunnel F</u> <u>Run No.</u>	<u>M<sub>∞</sub></u>	<u>Re<sub>∞,ℓ</sub></u> <u>x 10<sup>-6</sup></u>	<u>α,</u> <u>deg</u>	<u>α<sub>g</sub>,</u> <u>deg</u>	<u>φ,</u> <u>deg</u>	<u>δ<sub>e</sub>,</u> <u>deg</u>	<u>δ<sub>BF</sub>,</u> <u>deg</u>	<u>δ<sub>SB</sub>,</u> <u>deg</u>	<u>Model</u> <u>Position</u>
4998	20.5	0.11	30	30	0	0	0	0	Upright
4999	20.5	0.11	↓	-30	180	↓	↓	↓	Inverted
5000	17.9	0.34	↓	-30	180	↓	↓	↓	Inverted
5001	18.3	0.32	↓	30	0	↓	↓	↓	Upright
5003	20.3	0.08	↓	↓	↓	↓	↓	↓	↓
5004	18.7	0.38	↓	↓	↓	↓	↓	↓	↓
5005	18.3	0.12	↓	↓	↓	↓	↓	↓	↓
5006	18.6	0.11	↓	-30	180	↓	↓	↓	Inverted
5012	18.6	0.27	↓	-30	180	↓	↓	↓	Inverted
5008	19.3	0.11	30	30	0	15	16.3	0	Upright
5009	18.4	0.29	↓	30	0	↓	↓	↓	Upright
5010	18.9	0.11	↓	-30	180	↓	↓	↓	Inverted
5011	18.3	0.30	↓	-30	180	↓	↓	↓	Inverted
5002	18.1	0.33	30	30	0	-40	-11.7	0	Upright

Table 2. 0.010-Scale Orbiter Reference Dimensions

Note: Rockwell model designation is 51-0.

(TEST OA160)

<u>Parameter</u>	<u>Full Scale</u>	<u>Model Scale</u>
Reference Area (S <sub>ref</sub> )	2690.0 ft <sup>2</sup>	38.736 in. <sup>2</sup>
Reference Length (ℓ <sub>ref</sub> )	474.8 in.	4.748 in.
Reference Span (b <sub>ref</sub> ) (wing span)	936.7 in	9.367 in.
Moment Reference Center XMRP	841.7 in.	8.417 in.
Z	375.0 in.	3.750 in.
Body Length (ℓ)	1290.3 in.	12.903 in.
Base Area (A <sub>b</sub> )	421.7 in. <sup>2</sup>	6.072 in. <sup>2</sup>

Table 3. Summary of Tunnel Conditions

Run No.*	Time, msec	$P_0$ , psia	$T_0$ , °R	$\dot{q}_0$ , Btu/ft <sup>2</sup> -sec	$P_0'$ , psia	$p_\infty \times 10^3$ , psia	$\rho_\infty \times 10^6$ , slugs/ft <sup>3</sup>	$q_\infty$ , psia	$V_\infty$ , ft/sec	$M_\infty$	$Re_\infty, \ell \times 10^{-6}$	$\bar{V}_\infty$
4998	94	4843	5171	42.1	0.32	0.588	0.668	0.17	8619	20.5	0.11	0.057
4999	90	4631	5123	40.5	0.31	0.559	0.643	0.16	8573	20.5	0.11	0.058
5000	70	8839	4977	78.6	1.21	2.92	2.61	0.65	8466	17.9	0.34	0.029
5001	90	8142	4711	66.5	1.01	2.31	2.31	0.54	8214	18.3	0.32	0.030
5002	90	8210	4782	70.0	1.08	2.52	2.42	0.58	8281	18.1	0.33	0.029
5003	110	3950	5513	41.1	0.26	0.481	0.503	0.14	8914	20.3	0.08	0.067
5004	100	6999	3969	48.7	0.87	1.92	2.41	0.49	7477	18.7	0.38	0.028
5005	60	3749	5142	47.8	0.42	0.966	0.891	0.23	8568	18.3	0.12	0.049
5006	60	3603	5190	45.9	0.38	0.849	0.794	0.20	8612	18.6	0.11	0.052
5008	80	2997	4606	33.4	0.28	0.578	0.666	0.15	8067	19.3	0.11	0.055
5009	80	6944	4572	58.3	0.85	1.91	2.01	0.45	8071	18.4	0.29	0.032
5010	80	3082	4757	37.1	0.32	0.680	0.724	0.17	8209	18.9	0.11	0.054
5011	60	8121	4896	69.5	1.00	2.28	2.19	0.53	8387	18.3	0.30	0.031
5012	90	6439	4519	53.9	0.75	1.67	1.81	0.40	8016	18.6	0.27	0.034

\*See Table 1 for model test attitude and configuration.

Table 4. Summary of Aerodynamic Coefficients

<u>Run No.*</u>	<u>Time, msec</u>	<u>C<sub>N</sub></u>	<u>C<sub>m</sub></u>	<u>Xcp<sub>N</sub>/ℓ</u>	<u>C<sub>A</sub></u>	<u>C<sub>D</sub></u>	<u>C<sub>L</sub></u>	<u>L/D</u>
4998	94	0.856	-0.0371	0.666	0.152	0.559	0.666	1.19
4999	90	0.798	-0.0293	0.663	0.164	0.541	0.609	1.13
5000	70	0.774	-0.0254	0.662	0.105	0.478	0.618	1.29
5001	90	0.756	-0.0215	0.660	0.110	0.473	0.600	1.27
5002	90	0.722	0.0249	0.637	0.111	0.457	0.570	1.25
5003	110	0.776	-0.0289	0.664	0.179	0.543	0.583	1.07
5004	100	0.763	-0.0174	0.658	0.100	0.468	0.611	1.31
5005	60	0.841	-0.0396	0.667	0.151	0.551	0.653	1.18
5006	60	0.838	-0.0349	0.665	0.147	0.546	0.652	1.19
5008	80	0.895	-0.1170	0.698	0.173	0.597	0.689	1.15
5009	80	0.900	-0.1230	0.700	0.144	0.575	0.708	1.23
5010	80	0.903	-0.1220	0.700	0.170	0.599	0.697	1.16
5011	60	0.895	-0.1200	0.699	0.136	0.565	0.707	1.25
5012	90	0.754	-0.0222	0.661	0.111	0.473	0.598	1.26

\*See Table 1 for model test attitude and configuration.

## NOMENCLATURE

$A_b$	Base area, in. <sup>2</sup>
$b_{ref}$	Reference span, 9.367 in.
$C_A$	Forebody axial-force coefficient, $C_{A_t} - C_{A_b}$
$C_{A_b}$	Base axial-force coefficient, $[(p_\infty - p_B)/q_\infty] A_b/S_{ref}$
$C_{A_t}$	Total axial-force coefficient, $F_{A_t}/q_\infty S_{ref}$
$C_D$	Drag force coefficient in the stability axis system, $C_A \cos \alpha + C_N \sin \alpha$
$C_L$	Lift force coefficient (stability or wind axis), $C_N \cos \alpha - C_A \sin \alpha$
$C_m$	Pitching-moment coefficient about Sta 10.767, pitching moment/ $q_\infty S_{ref} \ell_{ref}$
$C_N$	Normal-force coefficient in the body axis system, $F_N/q_\infty S_{ref}$
$C_\omega$	Chapman-Rubesin viscosity coefficient, $(\mu_w/\mu_\infty)(T_\infty/T_w)$
$F_{A_t}$	Total axial force, lb
$F_N$	Normal force, lb
$F_{N_A}$	Normal-force component measured at aft normal-force gage location, lb
$F_{N_F}$	Normal-force component measured at forward normal-force gage location, lb
$H$	Enthalpy
$L/D$	Lift-to-drag ratio, $C_L/C_D$ (stability axis system)
$\ell$	Model length, 12.903 in.
$\ell_{ref}$	Reference length, 4.748 in.
$M_\infty$	Free-stream Mach number
$p_B$	Model base pressure, psia
$p_o$	Reservoir pressure, psi

$p'_0$	Total pressure behind normal shock in test section, psia
$p_\infty$	Free-stream static pressure, psia
$\dot{q}_0$	Stagnation heat-transfer rate on 1.0-in.-diam probe, Btu/ft <sup>2</sup> -sec
$q_\infty$	Free-stream dynamic pressure, psia
$Re_{\infty, \ell}$	Reynolds number based on free-stream conditions and model length
$Re_{\infty}/ft$	Reynolds number based on free-stream conditions and 1-ft length
$S_{ref}$	Reference area, 38.736 in. <sup>2</sup>
$T_0$	Reservoir temperature, °R
$T_w$	Model surface temperature, °R
$T_\infty$	Free-stream temperature, °R
t, TIME	Time, msec
V	Velocity, ft/sec
$V_\infty$	Free-stream velocity, ft/sec
$\bar{V}_\infty$	Hypersonic viscous parameter, $M_\infty \sqrt{C_m} / \sqrt{Re_{\infty, \ell}}$
$X_{cpN}/\ell$	Center-of-pressure location, $[0.65 - (C_m \times \ell_{ref}) / (C_N \times \ell)]$ measured from inner mold line (see Fig. 4)
Z	Vertical coordinate of model axis system (see Fig. 4)
$\alpha$	Angle of attack, deg
$\alpha_s$	Sector angle of attack, deg
$\delta$	Control surface deflection angle, deg; positive deflections are as follows: $(\delta_e)$ Elevator, trailing edge down $(\delta_{BF})$ Body flap, trailing edge down $(\delta_{SB})$ Speed brake, deflected out from the vertical stabilizer centerline, $\delta_{SB}$ is the included angle.
$\mu_w$	Viscosity at wall temperature

- $\mu_{\infty}$  Free-stream viscosity  
 $\rho_{\infty}$  Free-stream density, slugs/ft<sup>3</sup>  
 $\phi$  Model roll angle, deg

### **MOMENT REFERENCE**

- XMRP** Moment reference point on x-axis (XMRP = 8.417 in. from nose)  
**YMRP** Moment reference point on y-axis (YMRP = 0)  
**ZMRP** Moment reference point on z-axis (ZMRP = 0.25 in. below Z = 4.00)

### **SUBSCRIPTS**

- BF** Body flap  
**b** Base  
**e** Elevons  
**o** Reservoir  
**SB** Speed brake  
**ref** Reference conditions  
**w** Model wall conditions  
 **$\delta$**  Edge of boundary layer  
 **$\infty$**  Free-stream conditions

### **MODEL COMPONENTS: NASA/RI CONFIGURATION DESIGNATORS**

- B26** Orbiter body  
**C9** Canopy  
**E26** Elevon  
**F7** Body flap  
**M7** OMS pods  
**N28** OMS nozzle

R5 Rudder

V8 Vertical tail

W116 Wing

NOTE: The configuration designation is BCEFMNRVW.